Dean&Francis
ISSN 2959-6157

Experimental and Simulation Study of Vehicle Backside Constant Jet Drag Reduction

Lufei Li, Yiming Zhao, Zhengyu Tian

Guangzhou Foreign Language School, Guangzhou, China

Abstract:

Vehicle back constant jet drag reduction is one of the current research hotspots. This study explores the effect and principle of constant jet drag reduction in the back of a vehicle by combining theoretical analysis, wind tunnel test, and numerical simulation with the Ahmed-like vehicle body model as the research object. The results show that the optimal jet position is at a certain distance in front of the transition line between the vehicle's slant back and straight back, the optimal jet velocity is near 0.5 times the vehicle speed, and the optimal jet angle is slightly upstream in the direction of the normal of the plane where the jet hole is located. In this study, the optimal jet position is position 4, the optimal jet velocity is 20 m/s, and the optimal jet angle is 120° (pointing upstream) from the slanting back. Under the above conditions, the constant jet at the back of the vehicle can reduce the aerodynamic drag by 7.5%. The principle of drag reduction by constant jet includes reducing the intensity of the vehicle wake vortex and changing the position of the vehicle wake vortex. The effects of pressure and wake flow field (velocity, vortex volume, turbulent kinetic energy) are shown, the optimal jet parameters are determined, and the principle of drag reduction by constant jet at the back of the vehicle is analyzed.

Keywords: Vehicle; Aerodynamic drag reduction; Constant jet; Wind tunnel test; Numerical simulation.

1. Introduction

It has been found that when the vehicle speed reaches 80 km/h, 75%—80% of the total resistance during travelling comes from aerodynamic resistance. Moreover, aerodynamic drag is proportional to the square of the car's travelling speed, so as the speed increases, the aerodynamic drag will increase significantly, and the fuel consumption used to resist the drag will also increase significantly. Therefore, researching vehicle aerodynamic drag reduction is one of the important ways to improve fuel efficiency and reduce emissions.

The current research on vehicle aerodynamic drag reduction can be divided into traditional and flow

ISSN 2959-6157

control. Traditional aerodynamic drag reduction focuses on the overall shape design of the vehicle. By influencing the development and separation of the vehicle boundary layer and reducing the vortex through the design of the streamlined shape, the differential pressure resistance of the vehicle can be effectively reduced[1]. Generally speaking, the slower and longer the slope of the vehicle tail is, the closer it is to the streamlined shape, the smaller the vortex in the tail is, and the lower the negative pressure of the vehicle is. However, the optimization space of traditional aerodynamic drag reduction measures has become smaller and smaller. At the same time, the streamlined design has a slender tail section, which cannot be utilized for this part of the design but only for pure drag reduction. In other words, a large amount of interior space must be sacrificed for a streamlined design. Compared to the former, flow control is a relatively new research direction. It is an aerodynamic drag reduction method that controls the flow field around the vehicle, and one of its main effects is to perturb the boundary layer of the vehicle and increase its turbulence. With higher turbulence, the boundary layer is more resistant to separation, thus suppressing separation and reducing drag. Flow control is further categorized into passive and active control. Passive drag reduction measures include adding attachments to the original model to influence the flow. In contrast to passive control, active control controls the flow field by injecting energy into the flow field, which has the advantages of no need to change the shape, good adaptability to the environment, and easily realizing closed-loop control, etc., and has received more and more attention in recent years.

Constant jet, as the name suggests, i.e., the airflow that does not change with time, is the basis of the current vehicle surface blowing and suction drag reduction and hot topics, which can provide the theoretical basis for the engineering application of vehicle surface blowing and suction, and is also the basis of the periodic jet drag reduction and swept jet drag reduction[2]. Surface-blowing suction drag reduction technology has not been developed for a long time, and there is still a lot of research space for the study of constant jets and a lot of space for enhancing the drag reduction effect of vehicles. In this study, the wind tunnel test and numerical simulation method will be used to take the Ahmed car body model as the research object to study the effect of the jet position, jet velocity, and jet angle of constant jet on the aerodynamic drag, and based on this study, to give the optimal solution for the constant jet parameters and its drag reduction effect. This study will provide a theoretical basis and data support for the future vehicle constant jet aerodynamic drag reduction technology and help the practical application and development of constant jet technology.

2. Research Framework

2.1 Research object

In this study, the slant-back Ahmed class vehicle body[3] is selected as the research object, with a slant-back angle of 25°, as shown in Fig. 1. Existing studies mostly use the Ahmed class body model to study the vehicle aerodynamic drag and its tail winding characteristics, which retains the main shape features that affect the vehicle aerodynamic drag.

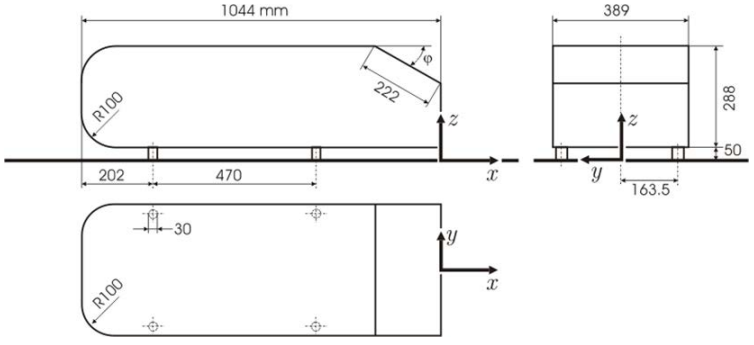

Fig. 1 Ahmed class body model

According to the shape of the back of the Ahmed class body model, the separation points may appear at the transition between the roof and the slanting back, as well as the transition between the slanting back and the straight back[3]. Therefore, in this study, five jet locations were set up in the back of the Ahmed class vehicle body model:

l Jet position 1: Located at the top of the vehicle, 48.625 mm from the transition line between the roof and the slant back.

l Jet Position 2: Located on the slant back of the vehicle, 48.625 mm from the transition line between the roof and the slant back.

l Jet Position 3: Located in the centre of the vehicle's slant back, 110 mm from the roof to the slant back transition line.

l Jet Position 4: At the vehicle's slant back, 48.625 mm

from the slant back to the straight-back transition line.
l Jet Position 5: Located on the straight back of the vehicle, 48.625 mm from the transition line between the slant back and the straight back.
Each jet position has five 7.78 mm diameter jet holes evenly spaced along the lateral (vehicle width) direction with a lateral spacing of 64.833 mm.

2.2 Research Problem

This study uses the Ahmed-mentioned vehicle body (see Fig. 2) as the research object. Using the research method combining wind tunnel test and numerical simulation, we study the effects of the jet position, jet velocity, and jet angle on the aerodynamic drag, surface pressure, and wake flow field of the vehicle and evaluate the effect of the constant jet on the drag reduction of the vehicle's backside. The framework of this study is shown in Figure 2.

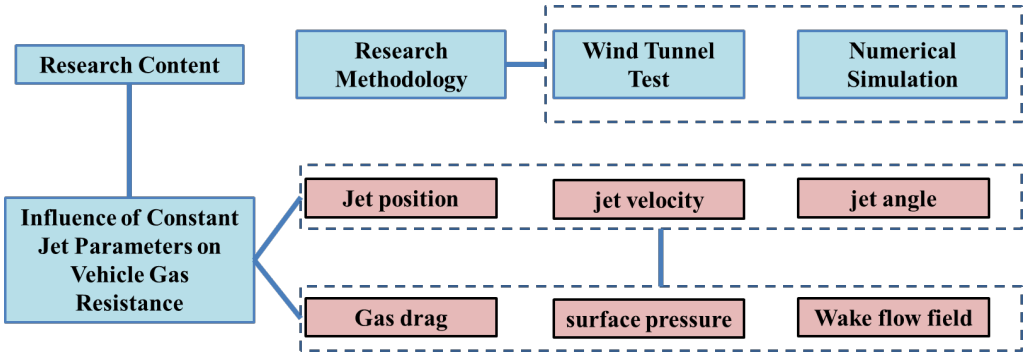

Fig. 2 Research Framework

3 Wind Tunnel Test

3.1 Test device

3.1.1 Homemade simple wind tunnel

To investigate the effect of constant jet on the drag of slant-back Ahmed vehicles and to simulate the flow field of real vehicles, we made a simple wind tunnel as shown in Fig. 3, which consists of four parts: A axial fan (610 mm in diameter), B contraction section (350 m in length), C rectification section (230 mm in length, 165 mm in width and height), D test section (1750 mm in length, 165 mm in width and height), and the starting position of the test section is 320 mm away from the front of the vehicle due to the limitation of the power of the test section, D test section (1750 mm long, 165 mm wide, 165 mm high), the starting position of the test section is 320 mm from the front end of the vehicle[4]. Due to the wind turbine power limitation, the average wind speed in the test section without the vehicle model is 5 m/s. The average wind speed of the test section without the vehicle model is 320 mm.

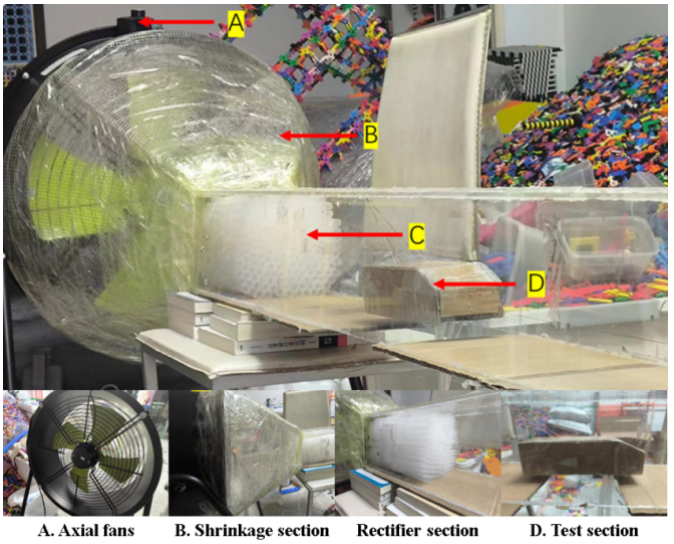

Fig. 3 Test setup in wind tunnel test

ISSN 2959-6157

3.1.2 Homemade model of slant-back Ahmed car body

The test model is a scaled-down model of the slant-back Ahmed body, with a scale of (80/389=) 0.206, as shown in Figure 4. The Ahmed body model is 214.70 mm long, 80 mm wide, 59.23 mm high, and has a slant-back angle 25°. The blockage ratio of the vehicle model is 17.4% (the ratio of the projected area of the vehicle model on the wind tunnel cross-section to the wind tunnel cross-sectional area).

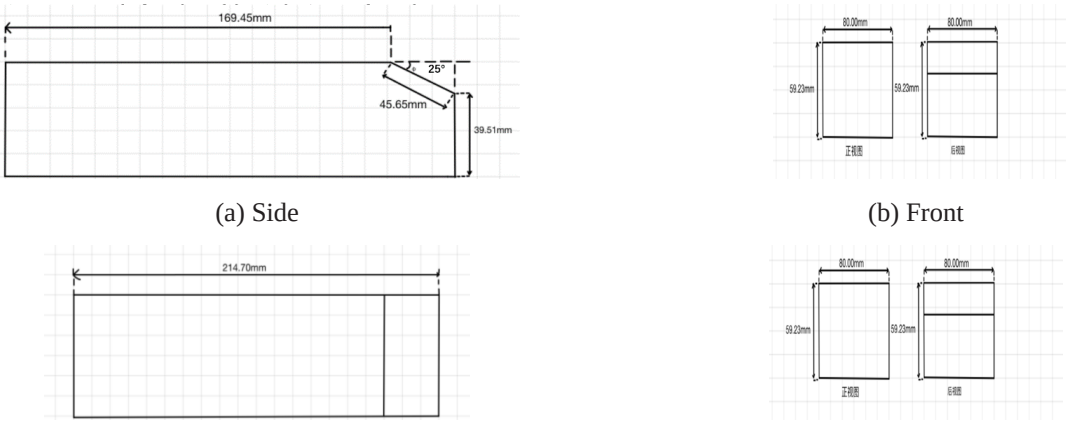

(a) Side (b) Front

(c) Topside (d) Backside

Fig. 4 Ahmed-like body model in wind tunnel test

3.1.3 Jet Generation Device

As shown in Figure 5, we arranged jet holes in the back of the vehicle model for the test and connected them to the air pump by a hose. During the test, the non-working jet holes were sealed with tape to prevent them from affecting the vehicle's rear winding. It should be noted that the hose extends from the bottom of the vehicle against the back and extends out of the wind tunnel, as shown in Fig.5, which may have some influence on the flow field at the rear of the vehicle.

Fig. 5 Physical drawing of the jet generation unit

3.2 Measurement methods

3.2.1 Pneumatic resistance measurement method

In the test, due to the vehicle model's small size and wind speed in the wind tunnel, the aerodynamic drag force on the vehicle is small, requiring extremely precise drag measurement equipment to measure the drag reduction effect of the constant jet. It is difficult to realize in a homemade simple wind tunnel test, and thus, the measurement method has become a difficult point in this wind tunnel test. In this wind tunnel test, we had to abandon the traditional method of using force sensors to directly measure the aerodynamic drag of the vehicle model. After a series of exploration processes (see Appendix A for the exploration processes), we proposed a method of measuring the drag reduction based on the travel of the model's single degree of freedom, a kind of indirect measurement method.

As shown in Figure 6, we placed a pulley at the wind tunnel exit and connected the vehicle body's rear part to a vertical weight. Measuring the height change of this weight can obtain the horizontal position change of the cart, thus reflecting the amount of change in the drag coefficient; the specific formula will be given later in the damping cross-section measurement method.

Fig. 6 Physical drawing of pneumatic resistance measuring device

This test will use the height change of the weight to indirectly measure the amount of change in the drag coefficient. As shown in Figure 7(a), the length of the two thin lines is known to be a fixed value; the length of the thin line of the suspension trolley is l. Assuming that the centre of mass of the trolley in the case of no blowing and the blowing case of the horizontal position of d_1, d_2, the vertical position of h_1, h_2, respectively, and hanging the trolley's thin line with the angle of the plumb line of the angle of the trolley and the θ_1, θ_2, respectively, the following relationship can be obtained:

$$\Delta h = \Delta d = d_1 - d_2 \tag{1}$$

$$\frac{d_1}{h_1} = \tan\theta_1, \frac{d_2}{h_2} = \tan\theta_2 \tag{2}$$

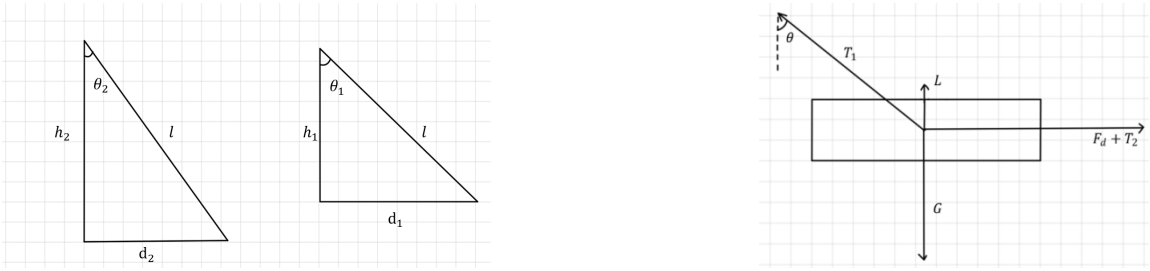

(a) Change of position (b) Force analysis

Fig. 7 Schematic diagram of vehicle model displacement and force analysis

Considering that in practice, the amount of change in the height of the cart is small enough to be ignored, then:

$$h_1 = h_2$$

Where h_1 is the difference in height between the fixed pulley and the top of the wind tunnel, the collation can be obtained.

$$\frac{\Delta h}{h_1} = \tan\theta_1 - \tan\theta_2 \tag{3}$$

According to Figure 7(b), for the force analysis of the trolley can be seen, the trolley subjected to gravity G, the lift force L from the two fine lines, respectively tension T_1, T_2, the trolley subjected to aerodynamic resistance F_d, as well as hanging the trolley fine line with the angle θ of the vertical direction to meet the following relationship:

$$G = T_1\cos\theta + L \tag{4}$$

$$F_d + T_2 = T_1\sin\theta \tag{5}$$

Since the lifting force L is much smaller than the other forces on the cart, we will ignore this term and Eq. (4) becomes:

$$G = T_1 cos\theta \tag{6}$$

Organize the formula (4), (5) can be obtained:

$$F_d + T_2 = G\tan\theta \tag{7}$$

Set the resistance of the cart without blowing and with blowing up as F_{d1} and F_{d2}, respectively, get:

$$F_{d1} + T_2 = G\tan\theta_1, F_{d2} + T_2 = G\tan\theta_2 \tag{8}$$

Then, it can be obtained that the decrease in the drag force on the cart is:

$$\Delta F_d = G(\tan\theta_1 - \tan\theta_2) \tag{9}$$

The formula (3) can be combined to obtain the relationship between the weight's height change and the drag reduction.

$$\Delta F_d = G\frac{\Delta h}{h_1} \tag{10}$$

The resistance coefficient is:

ISSN 2959-6157

$$C_d = \frac{2F_d}{\rho v^2 A} \tag{11}$$

The drag coefficient reduction is:

$$\Delta C_d = \frac{2\Delta F_d}{\rho v^2 A} \tag{12}$$

Due to the wind tunnel blockage ratio (17.4%) being larger, this wind tunnel test needs to carry out the blockage ratio correction; the ratio of the corrected drag coefficient C_{df} to the pre-correction drag coefficient C_d is:

$$\frac{C_{df}}{C_d} = \left(1 - x_B\right)^2 \tag{13}$$

Where: x_B is the wind tunnel blockage ratio.

The corrected drag coefficient reduction ΔC_{df} is as follows:

$$\Delta C_{df} = \left(1 - x_B\right)^2 \Delta C_d \tag{14}$$

According to the above analysis, the drag coefficient reduction can be obtained indirectly by measuring the change in weight height. In this test, we use Tracker video analysis modelling software to obtain the weight's height change.

The steps for video capture are as follows:

(1) Mark a point on the weight to record the height for video analysis, and make the plane where this point is located square to the camera.

(2) Start the fan and film the weight when the flow field stabilizes.

(3) After filming for at least 3 seconds, simultaneously start the air pump.

(4) After the flow field has stabilized, continue filming for another 3 seconds to end filming.

The video analysis steps are as follows:

(1) Set up a coordinate axis with a length scale with the vertical axis perpendicular to the ground according to the reference available within the video. In this test, the reference object is a cabinet in the video background, with one side perpendicular to the ground and one side horizontal to the ground, as shown in Figure 8. The magenta line in the figure is the coordinate axis; the blue line is the length scale, and the measured length of this section is 0.054 m. The length of this section is 0.054 m. The length of this section is 0.054 m.

(2) Set the marker on the weight as a mass, manually mark the position of the mass in the first three seconds and the last three seconds of the video (30 markings per second), and then export the height data of the mass. Figure 9 illustrates the change in height before and after marking the point on the weight when performing the analysis. Two pictures in the coordinate axis position are fixed: the left picture for the first marking point without jet state and the right picture for the last marking point with jet state. It is not difficult to see before and after the jet; there is a clear change in height.

(3) The first 90 and the next 90 height data are averaged, respectively, as the height of the weight in the jet-free condition and the height of the jet condition, and then subtracted to obtain the height difference Δh.

Fig. 8 Setting Axis and Length Scale

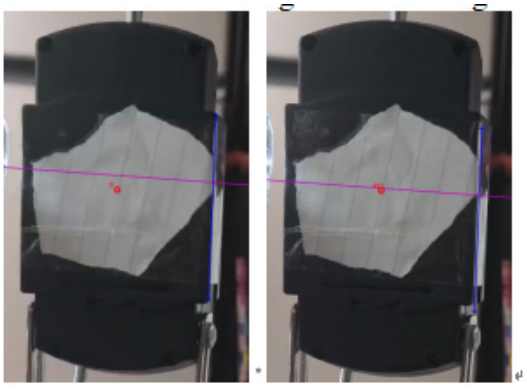

(a) Without jet (b) With jet state

Fig. 9 The height of heavy objects

3.2.2 Wind speed measurement method

An anemometer was used to measure the wind speed and jet velocity in this wind tunnel test. The range of the anemometer is 0.3 - 30 m/s.

3.3 Test conditions

At the time of the test, the air temperature at home was about 25°C, corresponding to an air density of 1.184 kg/m^3 and a dynamic viscosity of 1. 849×10^{-5} Pa·s. Based on the wind tunnel wind speed of 5 m/s and the vehicle height of 59.23 mm, the Reynolds number for this test was about 1. 896×10^4, and the Mach number was about 0.014.

(1) Jet position

The parameters of the jet position after scaling according to the model are as follows:

1. Jet position 1: located at the top of the vehicle, 1 cm

from the transition line between the roof and the slant back.
2. Jet position 2: Located at the slanting back of the vehicle, 1 cm from the transition line between the roof and the slanting back.
3. Jet Position 3: Located on the slant back of the vehicle, 2.25 cm from the transition line between the roof and the slant back.
4. Jet Position 4: Located at the vehicle's slant back, 1 cm from the transition line between the slant back and the straight back.
5. Jet Position 5: Located on the straight back of the vehicle, 1 cm from the transition line between the slant back and the straight back.
6. Each jet position has five 1.6 mm diameter jet holes evenly spaced along the lateral direction (vehicle width), with a lateral spacing of 1.5 cm.
(2) Jet velocity
In this test, since the air pump used in the test can only provide a jet of 3 - 8 m/s, we will test the following four jet velocities: 3 m/s (0.6 times the wind speed of the wind tunnel), 5 m/s (1 times the wind speed of the wind tunnel), 6 m/s (1.2 times the wind speed of the wind tunnel), and 8 m/s (1.6 times the wind speed of the wind tunnel). The desired wind speed can be obtained by adjusting the flow rate of the air pump and using an anemometer to check the wind speed at the nozzle.
(3) Jet direction
All jets will be shot in the direction normal to the plane where the jet hole is located.

3.4 Test Results

There is a big difference in both the value and the trend of the drag coefficient reduction under different jet position conditions:
1. Jet position 1: the drag coefficient reduction decreases first and then increases with jet velocity. In the interval from 0.6 times to 1.2 times the wind speed of the wind tunnel, the drag coefficient decreases gradually; however, there is a significant increase in 1.6 times the wind speed of the wind tunnel, and the maximum value is 0.043.
2. Jet position 2: The drag coefficient reduction decreases with the increase in jet velocity. The maximum value is 0.006 at 0.6 times the tunnel wind speed.
3. Jet position 3: the drag coefficient decreases with the increase of jet velocity in general, then decreases and then is unchanged. The maximum value is 0.066 at 1 times the wind speed in the wind tunnel.
4. Jet position 4: drag coefficient reduction with the increase in jet velocity increases, decreases, and is unchanged. The trend is similar to jet position 3, and the maximum value is 0.046 at 1 times the wind speed in the wind tunnel.
5. Jet position 5: the drag coefficient reduction increases and then decreases with the increase of jet velocity. There is a small increase in the drag coefficient reduction between 0.6 times the wind speed of the wind tunnel and 1 times the wind speed, with a peak value of 0.006, followed by a significant decrease.
It can be seen that, except for jet position 1, the optimal jet velocity of each other jet position is between 0.6 times and 1 times the wind speed of the wind tunnel, but there is still a big difference in the trend of the drag coefficient reduction with the increase of jet velocity under the conditions of each jet position.

4 Numerical Simulation

4.1 Simulation Setup

4.1.1 Vehicle Model

The model used in this numerical simulation is a slant-back Ahmed-like vehicle model, as shown in Figure 10, where the slant-back angle of the vehicle is 25°. The simulation takes the vehicle height (including struts) as the characteristic height H (= 0.338 m).

Fig. 10 Ahmed class vehicle body model

4.1.2 Computational area and boundary conditions

The distance of the vehicle model from the front face of the computational region is 8.7 H, the distance from the rear face of the computational region is 16.3 H, and the distance from the two side faces of the computational region is 8.3 H. The height of the computational region is 8.9 H. The obstruction ratio of the computational region is 0.6%. The front surface of the calculation area is set as velocity inlet, and the incoming wind speed is set to 40 m/s; the rear surface of the calculation area is set as pressure outlet, and the pressure is set to 0; the ground surface is set as no-slip fixed wall; the top surface and both sides of the calculation area are set as slip walls; the surface of the Ahmed class vehicle model is set as no-slip wall, and the jet hole is set as velocity inlet.
The air density is 1.225 kg/m^3, and the dynamic viscosity is 1. 802×10^{-5} Pa·s.

ISSN 2959-6157

Figure 11 illustrates the dimensionless distance y+ of the first colourful layer mesh on the vehicle model surface. The vehicle model surface y+ is near 5, which meets the requirements of the turbulence model chosen for this simulation.

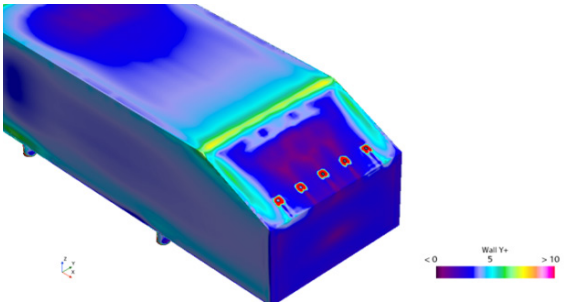

Fig. 11 Dimensionless distance of the first colourful layer mesh on the vehicle model surface

4.2 Simulation conditions

Based on the incoming wind speed of 40 m/s and the characteristic height of 0.338 m, the Reynolds number of this numerical simulation is 9. 191×10^5, and the Mach number is 0.117.

(1) Jet position: This numerical simulation adds five sets of jet holes based on the Ahmed class body model to create five positions.

(2) Jet velocity: Seven different jet velocities are set in this numerical simulation, which are 10 m/s (0.25 times the incoming wind speed), 15 m/s (0.375 times the incoming wind speed), 20 m/s (0.5 times the incoming wind speed), 25 m/s (0.625 times the incoming wind speed), 30 m/s (0.75 times the incoming wind speed), 35 m/s (0.875 times the incoming wind speed), 40 m/s (0.875 times the incoming wind speed), and 40 m/s (0.875 times the incoming wind speed). (0.875 times the incoming wind speed), 35 m/s (0.875 times the incoming wind speed), and 40 m/s (1 times the incoming wind speed). The jet velocity is constant throughout the simulation.

(3) Jet angle: Five different jet angles are set for this numerical simulation: 30° (pointing downstream), 60° (pointing downstream), 90°, 120° (pointing upstream), and 150° (pointing upstream) from the plane where the jet hole is located.

4.3 Simulation results

4.3.1 Effect of jet position on vehicle aerodynamic characteristics

(1) Vehicle aerodynamic drag

Figure 12 illustrates the relationship between the drag coefficient of the vehicle model and the jet position under the condition that the jet velocity is 0.5 times the incoming wind speed. The drag coefficient at jet position 4 is the smallest, 0.316, and the drag reduction rate is 7.1%.

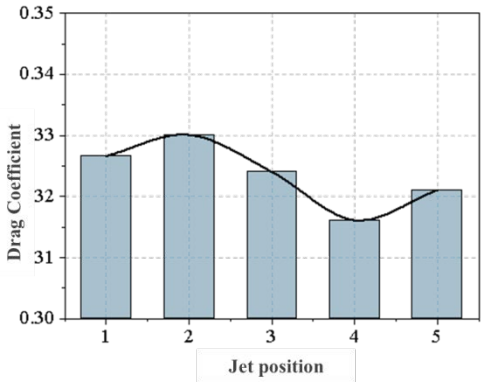

Fig. 12 Relationship between drag coefficient and jet position for jet velocity of 0.5 times the incoming wind speed

(2) Vehicle surface pressure

Figure 13 shows the pressure distribution of the vehicle surface under different jet positions (jet velocity is 0.5 times the incoming wind speed), and the figure also includes the case of no jet. There is an obvious negative pressure region at the transition between the vehicle's top and the slant back. This region in jet positions 1 and 2 is significantly more negatively pressurized and has a more chaotic pressure distribution than the other cases, probably because the jet close to this location disturbs the flow field. A smaller positive pressure region exists at the transition between the slant back and straight back of the vehicle and in the middle of the straight back. The area is more concentrated in the jet positions close to this area (Jet Position 4 and Jet Position 5), and the negative pressure is greater on both sides of the vehicle.

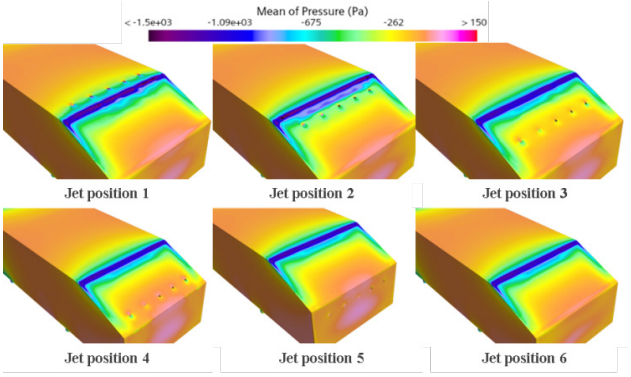

Figure 13 Surface pressure distribution of vehicle model under different jet position conditions

(3) Vehicle tail flow field

Figure 14 shows the velocity cloud of the vehicle tail

under different jet position conditions (the jet velocity is 0.5 times the incoming wind speed), and the figure also includes the case of no jet. There is an obvious low-speed vortex region behind the straight back of the vehicle, with two main vortices and flow separation occurs at the transition between the slant back and the straight back. When the jet position is on the slant back of the vehicle (jet position 2, jet position 3, and jet position 4), the boundary layer on the vehicle surface downstream of the jet orifice thickens. When the jet position is on the straight back of the vehicle (jet position 5), the jet moves the vortex away from the vehicle surface.

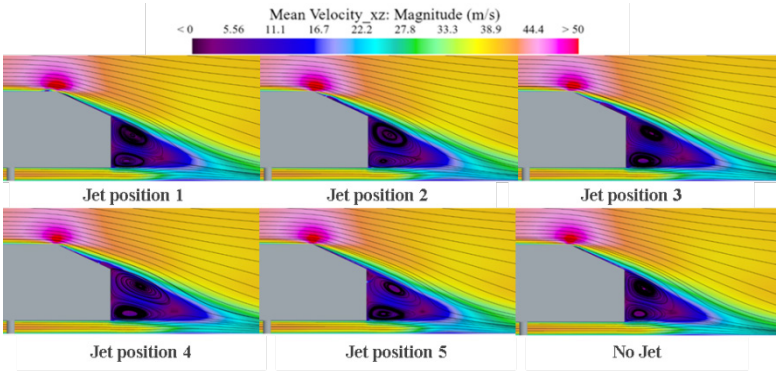

Fig. 14 Velocity distribution and streamlines at the rear of the vehicle model under different jet position conditions

4.3.2 Effect of jet velocity on vehicle aerodynamic characteristics

(1) Vehicle aerodynamic drag

For any jet position, the drag coefficient does not decrease monotonically with increasing jet velocity, but there exists an optimal jet velocity, and this velocity can be considered to be in the neighbourhood of 0.5 times the incoming wind speed. Figure 14 illustrates the minimum drag coefficient of the vehicle model under different jet position conditions. The drag coefficient is minimized at jet position 4 (jet velocity of 0.5 times the incoming wind speed) at 0.316, with a drag reduction of 7.1%. Considering that the optimal jet position is near 4, the effect of jet velocity on the vehicle surface pressure and wake flow field at this jet position is analyzed below.

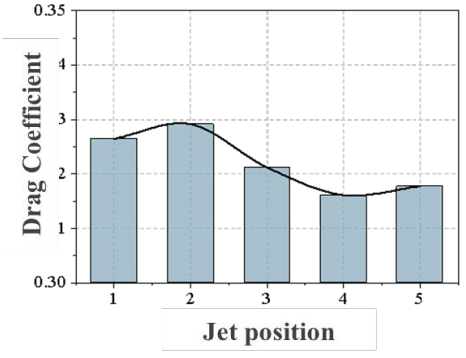

Fig. 15 Minimum drag coefficient of vehicle model under different jet position conditions

(2) Vehicle surface pressure

Figure 16 shows the surface pressure distribution of the vehicle model for different jet velocities (jet position 4). The pressure distribution and magnitude are very similar at each jet velocity: there is a clear negative pressure region at the transition between the roof and the slanting back and a smaller positive pressure region at the transition between the slanting back and the straight back, as well as in the middle of the straight back of the vehicle.

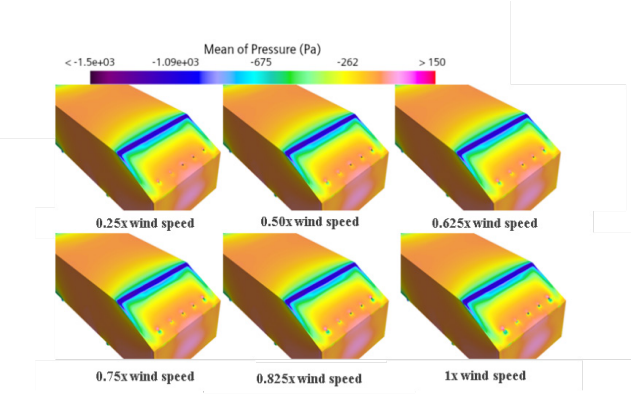

Fig. 16 Surface pressure distribution of vehicle model under different jet velocity conditions

(3) Vehicle tail flow field

Figure 17 shows the velocity cloud of the wake under different jet velocity conditions (jet position 4). The larger the jet velocity, the thicker the boundary layer on the vehicle surface downstream of the jet hole, indicating that the more significant the perturbation of the boundary layer.

ISSN 2959-6157

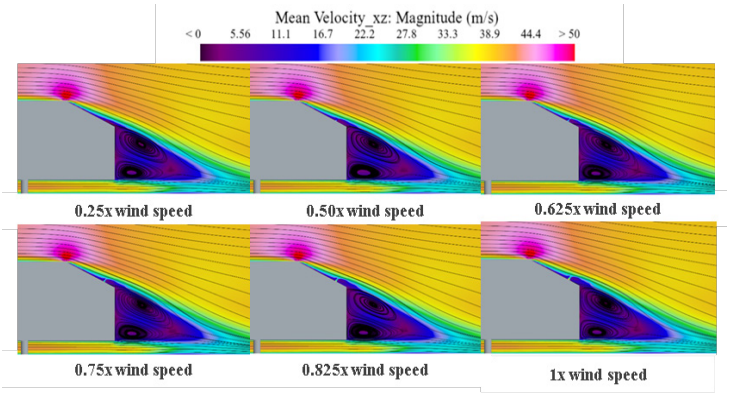

Fig. 17 Velocity distribution and streamlines in the wake of a vehicle model under different jet velocity conditions

4.3.3 Effect of jet angle on vehicle aerodynamic characteristics

(1) Vehicle aerodynamic drag

Figure 18 illustrates the relationship between the vehicle model's drag coefficient and the jet angle under the conditions of jet position 4 and a jet velocity of 0.5 times the incoming wind speed. The drag coefficient decreases and then increases with the increase of the jet angle and reaches a minimum value of 0.315 when the jet angle is 120°, and the drag reduction rate is 7.5%.

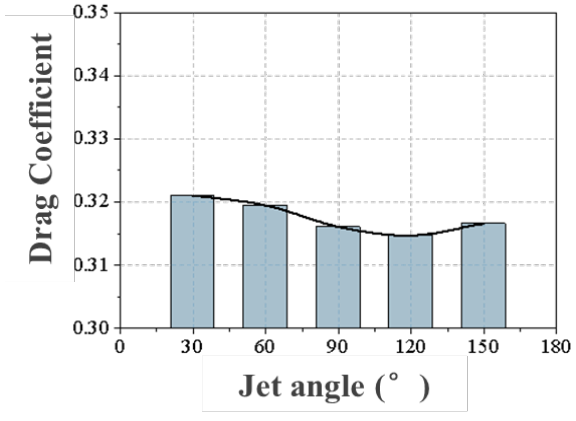

Fig. 18 Relationship between drag coefficient and jet angle

(2) Vehicle surface pressure

Figure 19 shows the pressure cloud of the vehicle model under different jet angles (jet position 4, jet velocity 0.5 times the incoming wind speed). It can be seen that the distribution of the pink region close to the location of the jet hole, i.e., the region with the least negative pressure, is biased in the direction in which the jet is biased. It indicates that the jet passing over the surface reduces the negative pressure on the surface. However, the areas of less negative pressure on the back of the vehicle do not show any significant change. Indicates that the jet passing over the surface reduces the negative pressure on the surface. However, the areas of less negative pressure on the back of the vehicle do not show any significant change.

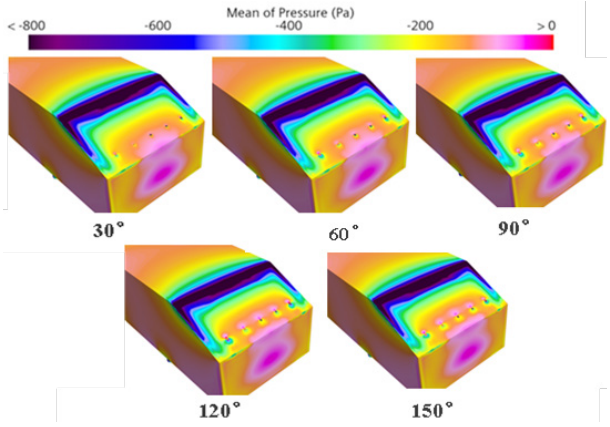

Fig. 19 Surface pressure distribution of vehicle model under different jet angle conditions

(3) Vehicle tail flow field

Figure 20 shows the velocity cloud of the vehicle model under different jet angles (jet position 4, jet velocity is 0.5 times the incoming wind speed). The thickness of the boundary layer downstream of the jet hole increases and then decreases with the increase of the jet angle, and the inflexion point occurs at the jet angle of 120°. That may be because here, close to the separation point, the direction of velocity in the boundary layer is no longer parallel to the surface of the vehicle but is biased toward the side away from the surface of the vehicle, and the jet angle of 120° is approximately perpendicular to it.

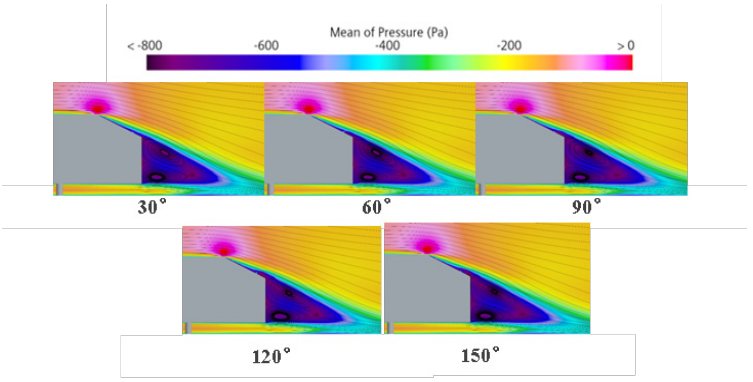

Fig. 20 Velocity distribution and streamlines at the rear of the vehicle model under different jet angle conditions

5 Conclusion

In this study, a combination of wind tunnel test and numerical simulation is used to investigate the effects of the position, velocity and angle of the constant jet on the aerodynamic drag of the vehicle behind the Ahmed class body model to determine the parameters of the jet with the optimal drag reduction effect and to explain the reason why the constant jet can realize the aerodynamic drag reduction. The main conclusions are as follows:

(1) The constant jet at the back of the vehicle can reduce drag, and the jet position, jet velocity and jet angle affect the drag reduction effect. The optimal jet position is at a certain distance in front of the transition line between the vehicles slanting back and straight back, the optimal jet velocity is near 0.5 times the vehicle's speed, and the optimal jet angle is slightly upstream in the direction normal to the plane where the jet hole is located.

(2) The constant jet at the back of the vehicle can reduce the aerodynamic drag by at least 7.5%. The drag coefficient of the vehicle model is 0.340 when there is no jet; the drag coefficient of the vehicle model is 0.315 under the above optimal jet parameters (jet position 4, jet velocity 20 m/s, jet angle 120°).

(3) The principles of drag reduction by the constant jet at the back of the vehicle are divided into two kinds: (i) disturbing the boundary layer on the vehicle surface, avoiding/delaying the separation of the boundary layer, and reducing the intensity of the vortex at the rear of the vehicle; and (ii) blowing away the vortex at the rear of the vehicle directly, increasing the distance between the vortex and the surface of the vehicle, and changing the position of the vortex at the rear of the vehicle. The first principle, dominated drag reduction, is more cost-effective.

The results of this wind tunnel test and numerical simulation show, to some extent, the effectiveness of the vehicle back constant jet drag reduction and illustrate the effect of jet position, jet velocity, and jet angle on the drag coefficient.

References

[1] He, D.H. Wind Engineering and Industrial Aerodynamics [M]. Beijing: National Defense Industry Press, 2006. 555-565.

[2] Wang Hongwei. My understanding of fluid dynamics [M]. Beijing: National Defense Industry Press, 2014. 162-168.

[3] Ahmed S R, Ramm G, Faltin G. Some salient features of the time-averaged ground vehicle wake[J]. SAE Transactions, 1984, 93(2): 473–503.

[4] Rossitto G, Sicot C, Ferrand V, et al. Influence of afterbody rounding on the pressure distribution over a fastback vehicle[J]. Experiments in Fluids, 2016, 57: 43.